JOURNAL OF CATALYSIS 64, 251–259 (1980)

Characterization of Reduced Natural Garnierite and Its Catalytic Activity for Carbon Monoxide Hydrogenation

PETER A. JACOBS AND HUBERT H. NIJS

Centrum voor Oppervlaktescheikunde en Colloïdale Scheikunde, Katholieke Universiteit Leuven, De Croylaan 42, B-3030 Heverlee, Belgium

AND

GEORGES PONCELET

Groupe dé Physico-Chimie Minérale et de Catalyse, Université Catholique de Louvain, 1 Place Croix du Sud, B-1348 Louvain-la-Neuve, Belgium

Received March 9, 1979; revised July 2, 1979

Natural garnierite, a nickel-containing mineral from New Caledonia, was reduced in hydrogen. The mineral and its reduced forms were characterized by X-ray diffraction, electron microscopy, and microprobe analysis. The reduction was followed volumetrically and the Ni^0 phase characterized by H_2 chemisorption. The catalytic activity of this mineral was determined in the hydrogenation reaction of carbon monoxide. Experiments were done in typical methanation and so-called Fischer–Tropsch conditions. The mineral consists of a mixture of a 10-Å phase (talc-like fluffy particles) and a 7-Å serpentine-like phase (fibers). The major amount of nickel is associated with the talc phase. Minor amounts are in the serpentine fibers and possibly substituted in the lattice of the minerals. Qualitative evidence for a redispersion of Ni in the serpentine fibers is advanced. At the moment this occurs, the turnover numbers of CO disappearance are optimum. Compared to other supports, they are considerably lower. The product distribution is within C_1–C_4 and follows closely a Schulz–Flory distribution.

INTRODUCTION

Ni-supported catlaysts are widely used for the synthesis of hydrocarbons from CO and H_2, in particular for the production of methane. In spite of the enormous amount of work already done in this area, there has been within the last years a remarked resurgence of interest for these reactions and for the solids catalyzing them. This is a consequence of the future problems expected to result from the shortage of oil and natural gas.

Several aspects of the reaction of methanation and Fischer–Tropsch synthesis have been the subject of recently published review articles. Mills and Steffgen (*1*) discussed the importance of synthetic methane, the mechanistic aspects of methanation, and the main methanation catalysts. Vannice (*2*) has put more emphasis on kinetics and adsorption. This author also summarized the different mechanistic models proposed for the reaction of CO, while Ponec (*3*) provided some arguments supporting a dissociative mechanism of CO for methanation and possibly for the Fischer–Tropsch synthesis.

Trimm (*4*) has mainly focused his attention on the problems of coke formation and removal from Ni catalysts. Considering only the Ni-supported catalysts, several papers published recently deal mainly with preparational aspects. They suggest that improvements of catalyst performances can still be expected by carefully controlling particular parameters involved in their preparation (*5–7*).

0021-9517/80/080251-09$02.00/0

Clay minerals have been used in the past as catalysts or catalyst supports. The acid-treated montmorillonite was used as a cracking catalyst. In recent years, a series of synthetic clay-based catalysts have been proposed as catalysts, e.g., the Ni-containing synthetic montmorillonite (SMM) of Granquist *et al.* (*8*) and the metal-substituted chrysotile of Robson (*9, 10*). These catalysts were shown to develop high activity, e.g., in hydrocracking and hydroisomerization of *n*-paraffins (*11*) and even in methanation (*12*). The use of clay minerals as catalysts has been reviewed by Swift (*11*).

Naturally occurring Ni-bearing silicates have been known for some time by clay mineralogists. Garnierite is the general name given to hydrous magnesium–nickel silicates, which in many cases consist of intimate mixtures of 1 : 1 (serpentine or chrysotile type) and 2 : 1 (talc-like) components (*13*). In terms of overall chemical composition reduced garnierites may be considered as Ni/MgO–SiO_2 catalysts.

This work aims to study the activation of natural garnierite and its use for the hydrogenation reaction of carbon monoxide in methanation and Fischer–Tropsch conditions.

EXPERIMENTAL

Material

The natural garnierite sample used in this work came from New Caledonia and showed a homogeneous pale green color. It was ground, pelletized, and crushed before use. Particles with a size of 140–180 μm were used in all experiments. The chemical composition (in weight percentage) determined by atomic absorption spectrometry was as follows:

Al_2O_3 = 0.10	CaO = 0.05	NiO = 16.75
Fe_2O_3 = 3.76	K_2O = 0.01	SiO_2 = 41.04
MgO = 25.04	Na_2O = 0.03	H_2O = 13.22.

Methods

X-Ray diffraction. X-Ray diffractograms were obtained on a Philips instrument, using the Ni-filtered CuKα line. The scanning speed per minute was $2\theta = 1°$.

Thermoanalysis. TGA, DTG, and DTA curves were obtained simultaneously on a Mettler Thermoanalyzer between 300 and 1273 K, using a heating rate of 8 K/min. Inert Al_2O_3 was used as reference. Runs were done under helium and hydrogen at a flow rate of 2.22 ml s^{-1}.

Electron microscopy and microprobe analysis. Transmission electron microscope (AEI EM6G equipment) and microprobe analyses (JEOL TEMSCAN 100 C instrument, fitted with an energy dispersion spectrometer (EDS)) were also used to characterize the sample of garnierite.

Volumetric measurements. Temperature-programmed reduction (TPR) and reoxidation (TPO) were done in a low-volume all-glass recirculation reactor. This circuit consisted of a high-speed piston pump, a reactor, a cold trap, and a Bell and Howell Type 4-326 pressure transducer (0.2% accuracy). Hydrogen chemisorption was carried out in the same instrument. One gram of sample was used in these experiments.

Catalytic measurements The rates of CO hydrogenation and product distributions were determined in a continuous-flow reactor, operating in the differential mode at low conversions. The catalyst bed was 8 × 4 mm (diameter × depth). Product analysis was done on-line, using a Hewlett Packard 5830 reporting gas chromatograph equipped with TC and FID detectors. The columns used were a 1-m Chromosorb 105 adsorption column for separation of CO, CO_2, and C_1–C_5 hydrocarbons, and 1 100-m 0V101 capillary column for the higher hydrocarbons.

RESULTS AND DISCUSSION

Physicochemical Characterization of the Garnierite Sample and Its Reduced Forms

X-Ray diffraction data. The X-ray dif-

fractogram of garniertie (Fig. 1A) shows the lines of a serpentine-like mineral together with a talc-like mineral, with basal spacing of 7 and 10 Å, respectively. Quartz is present as an impurity.

Reduction below 673 K (Figs. 1B and 1C) hardly affects the basal reflection of the 7-Å and 10-Å phases, while the quartz diffraction lines increase in intensity. A hydrogen treatment at 773 K (Fig. 1D) appreciably reduces the band intensities of the serpentine-like material, while the 001 diffraction line of the 10-Å phase remains unaffected. At the same time, a broad band (2θ = 44.5) due to metallic Ni starts to develop.

After reduction at 873 K (Fig. 1E), the lines of the 7-Å phase have vanished, while the [001] reflection of the 10-Å phase is still weakly visible. The two main lines of metallic Ni (2θ = 44.5 and 51.8°) are strongly developed. At the same time, two new bands appear near 14.7 and 25 °A (i.e., 2θ = 3.53 and 6.01, respectively). This also is observed by other authors (*14*), after heat

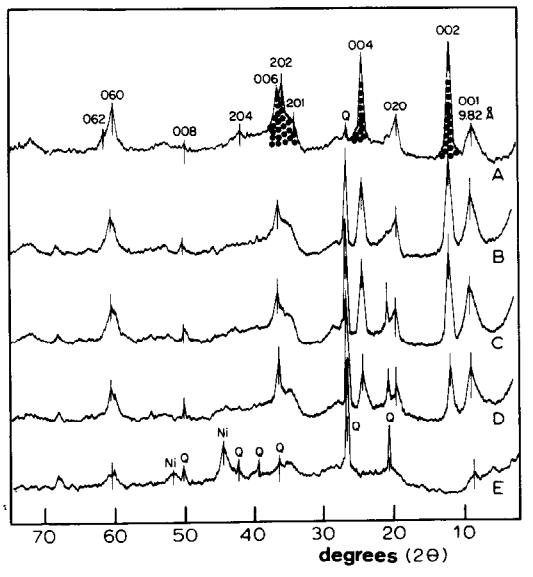

FIG. 1. X-Ray diffractograms of garnierite: orginal sample (A) after hydrogen reduction at 573 (B), 673 (C), 773 (D), and 873 K (E). 10-Å phase = 001 reflection; 7-Å phase = 002, 004, 201, 202, and 006 relfections; reflections common to both phases = 020, 060.

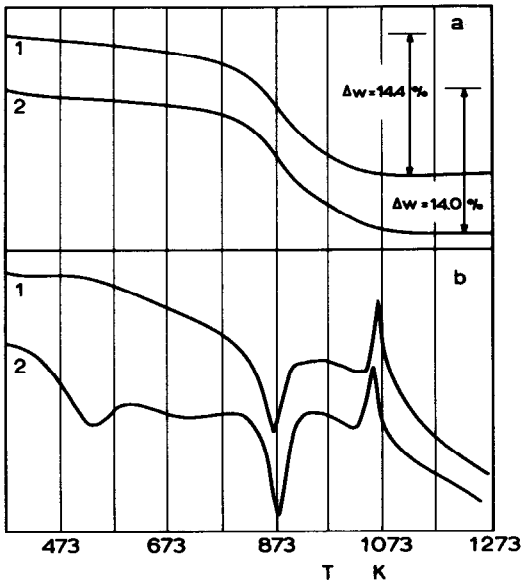

FIG. 2. Thermoanalytical curves of garnierite in a hydrogen (1) or helium (2) atmosphere: (a) weight loss and (b) DTA curves.

treatment above 843 K of nickel-rich garnierite. The explanation for this behavior could be the formation of a disordered phase (*14*).

Thermoanalysis of the garnierite sample. TGA curves obtained under He and H_2 are shown in Fig. 2a. The total weight loss is almost 14% in each atmosphere. Below 773 K the sample weight loss is only around 3%. The main weight changes occur between 773 and 1073 K and correspond to the dehydroxylation of the 7-Å serpentine-like mineral and possibly also of the 10-Å talc-like phase. The corresponding DTA curves are given in Fig. 2b. An endothermic peak at 543 K under helium is due to dehydration–dehydroxylation of an amorphous Ni-oxide–Ni-hydroxide phase (*15*). Under H_2 this peak is absent due to overlap with an exothermic effect resulting from NiO reduction. The endotherm near 873 K due to the dehydroxylation of the 7-Å phase and probably also of the 10-Å mineral is followed by an exotherm caused by recrystallization into olivine (*14*).

Electron microscopy and microprobe analysis. Samples of the initial and of the

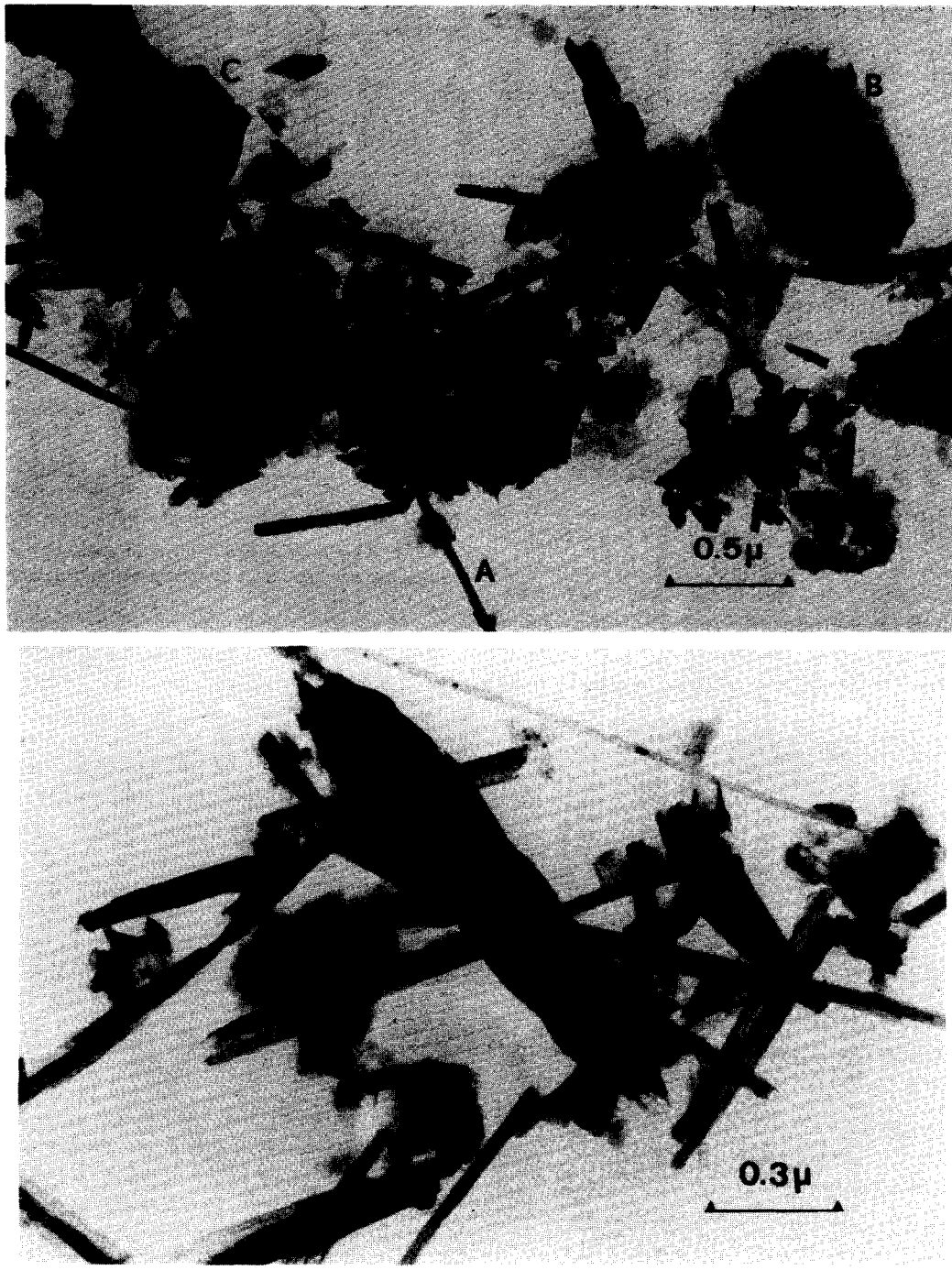

FIG. 3. Electron micrograph of natural garnierite (top) and after reduction at 773 K (bottom). (A) A fiber; (B) a fluffy particle; and (C) a kaolinite-type particle.

reduced garnierites have been examined by transmission electron microscopy (TEM). The 7-Å phase appears as elongated fibers (A), much like those of chrysotile, while the

10-Å mineral is made of fluffy particles (B) (Fig. 3). Microprobe analyses made on several particles belonging to the two types of morphology clearly showed (Fig. 4) that Ni is not homogeneously distributed between the two silicates. Ni is almost absent in the 7-°A phase mineral (fibrous component), but is mainly associated with the fluffy particles (10-Å mineral).

The electron micrographs show that upon reduction at 573 K Ni metal particles start to appear on the 10-Å phase (average diameter = 5–6 nm). When the garnierite is reduced at higher temperatures, the size of the particles increases. Only after a 773 K reduction are metal particles visible within the chrysotile fibers, in the form of small plugs (5 × 12 nm) (Fig. 3 (bottom)). At the same time the number and the size of the Ni particles on the 10-Å mineral further increase (up to 20 nm). The electron micrographs of the sample after reduction at different temperatures have been published and discussed in detail elsewhere (*15*).

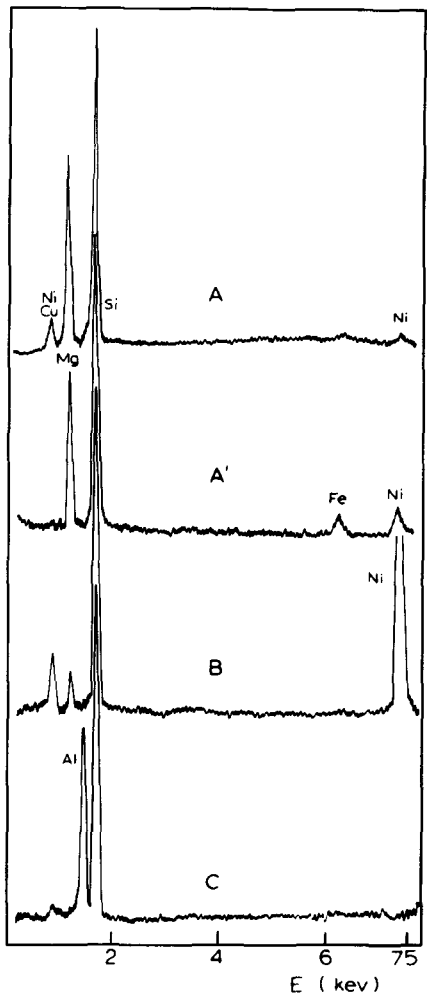

FIG. 4. Microprobe analyses on garnierite: (A) on a fiber and (B) on a fluffy particle: (A') on a fiber after reduction at 773 K; (C) on kaolinite-type particle.

Conclusions. The physicochemical experiments qualitatively give more information on the behavior of natural garnierite during a hydrogen reduction.

(i) The original sample mineralogically contains serpentine-like and talc-like phases and minor amounts of quartz. The serpentine phase (7 Å) morphologically has a tubular form like chrysotile and contains only a few nickel ions. The fluffy talc-like particles contain most of the nickel as an amorphous nickel oxide–hydroxide phase. Dehydroxylation of the two minerals starts above 823 K, while recrystallization into olivine occurs above 1023 K.

(ii) During the hydrogen activation above 673 K, the two minerals decompose. the talc-like mineral represents the more stable phase.

(iii) Nickel metal particles first appear in the talc-like phase and finally Ni is found as plugs in the serpentine-like fibers. Qualitatively this may indicate either a migration of Ni^0 from outside toward the tubular pores of serpentine or a sintering of the small amount of Ni initially present in the fibers, substituted in the lattice for Mg or in the pores as amorphous material.

Chemical Characterization of Natural Garnierite and Its Reduced Forms

Reduction–oxidation cycles. The rate of reduction in hydrogen of natural garnierite during a TPR experiment is given in Fig. 5. Three maxima in the rate of hydrogen uptake (trace a) show that three distinct Ni species are present in the original garnierite. The TEM and microprobe results

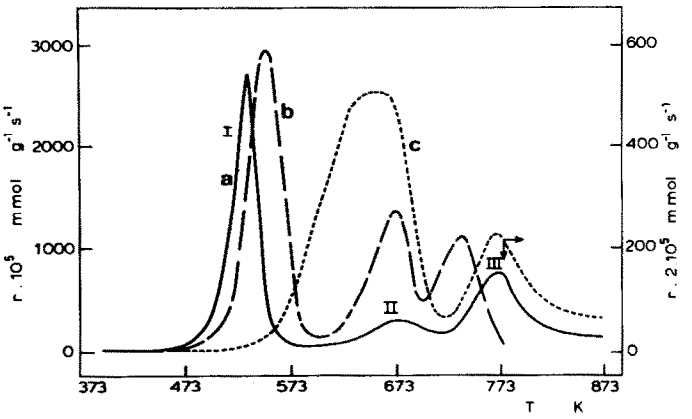

FIG. 5. Temperature-programmed reduction (a), reoxidation (b), and second reduction (c) of natural garnierite.

strongly suggest that the first maximum is associated with the talc-like phase and corresponds to the reduction of an Ni-oxide–hydroxide phase physically adsorbed on the talc-like crystals.

The broad and intermediate maximum of weak intensity is found in a temperature region slightly higher than expected for the reduction of bulk nickel oxide (see trace c, first maximum; for its assignment see below). This maximum may therefore be due to the reduction of minor quantities of Ni present in the serpentine pores, which are associated with deposits of amorphous silica. It is well known that interaction of silica with Ni decreases the reducibility of Ni (*16, 17*). This kind of Ni metal upon sintering may give rise to the plug-like Ni crystals observed after reduction at 773 K (Fig. 3). The third maximum is only observed when the minerals start to decompose (see thermogravimetric results of Fig. 2), just before the sudden dehydroxylation of the lattice hydroxyls occurs. Therefore the third maximum may be assigned to the reduction of lattice-substituted Ni ions, which are liberated only when the crystallinity of the material declines. This kind of Ni is for the major part present in the talc-like mineral.

The nickel metal formed is also reoxidized (trace b) in three distinct temperature regions. When the reduced sample is held in hydrogen at high temperatures (873 K, as done during the first TPR experiment), severe sintering may be expected. The plug-type Ni particles encaged in the serpentine fibers are expected to better resist oxidation than the Ni crystallites associated with the talc phase. The metal coming from reduction of lattice-substituted Ni ions is assumed to be intercalated between the mineral layers and as a result is oxidized only at high temperatures. The relative increase of the intermediate TPO peak compared to the TPR trace cannot be accounted for by sintering of the small amount of Ni coming from the serpentine phase. Therefore, as suggested already by the electron micrographs, redispersion of Ni crystallites has to occur in the serpentine fibers.

The second TPR trace shows that severe sintering occurs in oxygen. The first maximum has disappeared and Ni–O species are reduced at the temperature where bulk NiO is reduced.

Hydrogen chemisorption on Ni⁰. Samples of the parent garnierite were reduced for 1 h at the temperatures indicated. Reduction temperatures were selected in such a way that three samples contain the Ni^0 species I, I + II, and I + II + III, respectively (see Fig. 5). The surface area of the

TABLE 1

Characterization of the Nickel Metal Phase of Reduced Garnierite by Hydrogen Chemisorption

Reduction temperature (K)	Degree of reduction	$\frac{H^a}{Ni^0}$
623	0.365	0.30
673	0.402	0.35
723	0.574	0.12

[a] H_2 chemisorption at 300 K.

Ni metal phase in each case is given in Table 1, together with the degree of reduction. It is clear that upon increasing the reduction temperature, more Ni comes to the metallic state.

The dispersion of the metal phase with increasing reduction temperature is expected to decrease monotonically. However, the data of Table 1 show an optimum value at intermediate reduction temperature. This can be the result of a redispersion process, which already was invoked previously.

Conclusions. The hydrogen activation of natural garnierite results in the reduction of three different Ni forms: oxidic Ni associated with the talc phase, Ni oxide in interaction with occlusions in the serpentine fibers, and lattice-substituted nickel ions. Their reducibility decreases in the same order. Semiquantitatively, it is clear that redispersion of Ni metal has to occur, as a result of a migration of Ni from bulky crystallites to the serpentine fibers. As a consequence a reduction temperature for optimum Ni dispersion exists.

Catalytic Characterization of Reduced Garnierite: Carbon Monoxide Hydrogenation

Methanation of carbon monoxide. Pertinent data on the kinetic behavior of CO methanation in a hydrogen-rich feed and at atmospheric pressure over reduced garnierite are shown in Table 2. The activation energy and orders in the reactants are very close to those reported by Vannice (*18*) for Ni on alumina. The order in hydrogen is very high, while a negative order for CO is obtained. The turnover values for CO hydrogenation under the same conditions are also given. Here again, an optimum value is observed at intermediate reduction temperatures. This shows that when Ni metal is redispersed in the serpentine fibers and before it sinters to the plug shape, the Ni metal keeps a particularly favorable size in these pores. Since the system is very complex, it is difficult to attribute this to a particle size effect or to a support effect.

Even if CO is hydrogenated with less

TABLE 2

Kinetic Parameters for CO Hydrogenation at 573 K on Natural Garnierite

Reduction temperature (K)	H_2/CO	Reactant pressure (MN m^{-2})	E_A (kJ/mol) (500–573 K)	X[a]	Y[a]	$N \times 10^{3}$[b] (s^{-1})
623	3	0.101	97.8	1.80	−0.45	0.08 (0.07)[c]
673	3	0.101	111.0	1.80	−0.40	6.99 (7.01)
723	3	0.101	105.0	1.70	−0.47	1.18 (1.17)
573	1.5	2.130				26.04 (33.1)
673	1.5	2.130				50.53 (58.2)
723	1.5	2.130				47.43 (37.5)

[a] $r = k\, p_{H_2}{}^{X}\, p_{CO}{}^{Y}$.

[b] Molecules CO hydrogenated per surface Ni^0 and per second.

[c] Turnover numbers determined using H_2 chemisorption data on the used catalyst.

hydrogen in the feed and at higher pressures, the same optimum reduction temperature still exists (Table 2). It becomes more pronounced when the metal surface is used which is obtained when the catalyst is operating at steady state.

Absolute values of N determined at 573 K can be compared with the turnover numbers of Vannice (*18*) determined at 548 K for a whole series of more classical supports. The latter values always are considerably higher, indicating that garnierite is not a good support. At the moment, it is difficult to advance any fundamental reason for the low preexponential factors encountered with this system. Indeed, the activation energies reported for supported nickel (*18*) are very close to our data.

Fischer–Tropsch products. When CO is hydrogenated in a rich hydrogen feed and at atmospheric pressure, the only carbon-containing product is CH_4. At elevated pressures (1.5 MN m^{-2}) and with an H_2/CO ratio of 1.5, other hydrocarbons are also found. However, no products with carbon number higher than C_4 can be detected, nor are oxygen-containing compounds in the product stream.

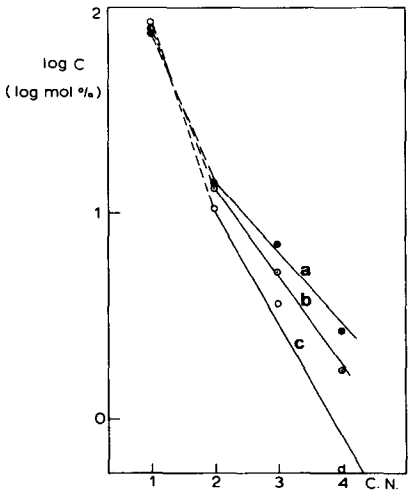

FIG. 6. Schulz–Flory distribution (C.N. = carbon number) of Fischer–Tropsch products over garnierite reduced at: (a), 573 (b) 673, and (c) 723 K.

TABLE 3

Olefin/Paraffin Ratios in the Products of CO Hydrogenation over Reduced Garnierite[a]

Reduction temperature (K)		Carbon number		
		C_2	C_3	C_4
573	—	0.47	2.16	1.94
673	—	0.40	1.41	1.39
723	—	0.09	0.50	0.05

[a] At 573 K; H_2/CO = 1.5; 2.13 MN m^{-2}.

The hydrocarbon concentration can be plotted according to the so-called Schulz–Flory equation (*19*). This is done in Fig. 6 for three reduction temperatures. This distribution of products corresponds to a "normal" distribution encountered in a polymerization reaction. For most of the catalysts for which a detailed product distribution is given, this kinetic law is followed from C_3 or C_4 onward (*19–21*). In each case, too much methane is found and not enough C_2 hydrocarbons. In the present case, the relation is much more satisfactory since the excess of C_1 formed has decreased and more C_2 is obtained. It is also seen that the higher catalyst reduction temperatures favor methane selectively. This behavior is typical for nickel.

The positive effect of low reduction temperatures is also observed when olefin/paraffin ratios in each carbon fraction are considered (Table 3). For each carbon number the olefin content decreases at the higher reduction temperatures. This cannot be due to an effect of conversion, since it is kept between 5 and 10%. However, since the system is very complicated and contains at least a bimodal distribution of metal particle sizes, it is impossible to assign this to a particle size effect or to a support effect. The C_3 fraction is most rich in olefins. Unfortunately, no detailed data exist for the moment for Ni on other supports, in order to show whether the latter behavior is typical for the garnierite support.

CONCLUSIONS

Reduced garnierties as support for Ni metal are less favorable than other supports in the hydrogenation of CO. An enhancement in activity due to the matrix appears at the moment redispersion of Ni occurs in the serpentine fibers and before this type of Ni sinters into plug-like particles. The kinetic parameters (orders in reactants and activation energy) are not substantially different from Ni on other supports.

The product distribution in Fischer–Tropsch conditions follows very closely a Schulz–Flory distribution, even at the lowest carbon numbers. Lower reduction temperatures give a more olefin-rich product.

ACKNOWLEDGMENTS

P.A.J. acknowledges a permanent research position as "Bevoegdverklaard Navorser" from N.F.W.O.–F.N.R.S. (Belgium). The authors thank the Belgian Government (Dienst voor Programmatie van het Wetenschapsbeleid) for financial support.

REFERENCES

1. Mills, G. A., and Steffgen, F., *Catal. Rev.* **8,** 159 (1973).
2. Vannice, M. A., *Catal. Rev.* **14,** 153 (1976); *Advan. Chem. Ser.* **163,** 15 (1977).
3. Ponec, V., *Catal. Rev. Sci. Eng.* **18,** 151 (1978).
4. Trimm, D. L., *Catal. Rev. Sci. Eng.* **16,** 155 (1977).
5. Kruissink, E. C., Alzamora, L. E., Orr, S., Doesburg, E. B. M., van Reijen, L. L., Ross, J. H. R., and van Veen, G., *in* "Proceedings, 2nd International Symposium, Scientific Bases Preparation Heterogeneous Catalysts, Louvain-la-Neuve, 1978," Preparation of Catalysts II, p. 143. Elsevier, Amsterdam, 1979.
6. Hermans, L. A. M., and Geus, J. W., Elsevier, Amsterdam, 1979. p. 113 of Ref. (*5*).
7. Richardson, J. T., Dubus, R. J., Crump, J. G., Desai, P., Osterwalder, U., and Cale, T. S., p. 131 of Ref. (*5*).
8. a. Granquist, W. T., U.S. Patent 3,252,757 (1966); b. Granquist, W. T., and Pollack, S. S., *Amer. Mineral.* **52,** 212 (1967). c. Wright, A. C., Granquist, W. T., and Kennedy, J. W., *J. Catal.* **25,** 65 (1972).
9. a. Robson, H. E., U.S. Patents (a) 3,729,429 (1972), (b) 3,804,741 (1973), (c) 3,848,018 (1974), (d) 3,850,746 (1974), (e) 3,852,165 (1974), (f) 3,868,316 (1975).
10. Sawyer, W. H., and Robson, H. E., U.S. Patent 3,838,041 (1974).
11. For a review: Swift, H. E., "Advanced Materials in Catalysis" (J. J. Burton and R. L. Garten, Eds.), p. 209. Academic Press, New York, 1977.
12. Kobylinski, T. P., and Swift, H. E., U.S. Patent 3,947,483 (1976).
13. Brindley, G. W., and Hang, P. T., *Clays Clay Miner* **21,** 27 (1973).
14. Hang, P. T., and Brindley, G. W., *Clays Clay Miner.* **21,** 51 (1973).
15. Poncelet, G., Jacobs, P. A., Delannay, F., Gerot, M., Gerard, P., and Herbillon, A., *Bull. Minéral.* **102,** 379 (1979).
16. Coenen, J. W. E., and Linsen, B. G., "Physical and Chemical Aspects of Adsorbents and Catalysts" (B. G. Linsen, Ed.), p. 471. Academic Press, New York, 1976.
17. Coenen, J. W. E., *in* "Proceedings, 2nd International Symposium, Scientific Bases Preparation Heterogeneous Catalysts, Louvain-la-Neuve, 1978," Preparation of Catalysts II, p. 89. Elsevier, Amsterdam, 1979.
18. Vannice, M. A., *J. Catal.* **37,** 449 (1975).
19. Henrici-Olivé, S., *Angew. Chem. Int. Ed.* **15,** 136 (1976).
20. Schulz, H., *Erdoel Kohle Erdgas Petrochem.* **30,** 123 (1977).
21. Vannice, M. A., *Advan. Chem. Ser.* **163,** 15 (1977).